

# High-Pressure Crystallisation of TiO<sub>2</sub> Nanocrystals

Dean C. Sayle\* and Thi X. T, Sayle

*DEOS, Cranfield University, Defence Academy of the United Kingdom, Shrivenham, Swindon, UK*

*\*Corresponding Author: [d.c.sayle@cranfield.ac.uk](mailto:d.c.sayle@cranfield.ac.uk)*

The full atomistic structure of a TiO<sub>2</sub> nanocrystal, about 7nm in size and comprising 16,000 atoms, has been generated using simulated melting and crystallisation, performed under high-pressure. Specifically, the nanoparticle was heated to 6000K after which the molten nanoparticle was crystallised at 2000K under 20GPa pressure. The resulting nanocrystal comprises rutile- and  $\alpha$ -PbO<sub>2</sub> - structured domains ( $\alpha$ -PbO<sub>2</sub> has been identified experimentally as a high-pressure phase of TiO<sub>2</sub>) expresses (111), (010), (001) and ( $\bar{1}\bar{1}0$ ) surfaces facilitating a polyhedral morphology and includes grain-boundaries and grain-junction. Molecular graphics images of the various microstructural features are presented together with snapshots of the crystallisation.

**Keywords:** Molecular dynamics, nucleation, growth, microstructure, polymorph,  
Interface

## 1. INTRODUCTION

The properties of a material can change dramatically as one traverses to the nanoscale. For example, in a previous simulation study<sup>1</sup>, we predicted that it was easier to extract oxygen from the surface of a CeO<sub>2</sub> nanocrystal (about 8nm in diameter) compared the (bulk) parent material<sup>2</sup>. This prediction was later confirmed experimentally by Mai and co-workers who measuring that ceria nanocrystals nanorods, nanopolyhedra and nanocubes are more reactive for CO oxidation compared with the bulk parent material<sup>3</sup>. This enhanced catalytic activity was attributed to the preferential exposure of thermodynamically ‘unstable’ surfaces, which are inherently more reactive towards CO oxidation, compared with more stable, yet less reactive, surfaces proffered by the parent material. Clearly, the ability to influence the morphology and hence the properties of nanomaterials is of considerable scientific and technological importance.

Many synthetic methods control shape and size via processing conditions for example: microwave-assisted solvothermal methods<sup>4</sup>, sol-gel techniques<sup>5</sup>, templating<sup>6</sup>, flame synthesis<sup>7</sup> etc. and new innovative techniques appear on a regular basis - generated from the enormous efforts focused on nanomaterials research. In this vein, a rather intriguing variable is the influence of very high pressures: ‘recently, high-pressure science has undergone a renaissance, with novel techniques and instrumentation, permitting entirely new classes of high-pressure experiments’<sup>8</sup> and spawning a wealth of new and prospective new materials<sup>9,10</sup>. Undaunted by the complexity and expense that plagues high-pressure experimentation, researchers have unraveled new insights into the somewhat profound materials behaviour at high pressures<sup>11</sup>. The challenges relating to equipment - gas gun<sup>12</sup>, diamond anvil<sup>13</sup> - and cost associated with high-pressure experimentation are not echoed in analogous high-pressure computational studies and therefore atomistic simulation provides an ideal forum in which one can explore the behaviour of materials at high-pressures to help complement experiment and

forms the basis of this present study. In particular, we investigate (simulate) the structure of  $\text{TiO}_2$  nanocrystals, generated via high-pressure crystallisation, starting from a molten precursor.

$\text{TiO}_2$  is an important material that has enjoyed a long history of study because of its photocatalytic and photovoltaic behaviour. Specifically, the material has the ability to convert light into chemical energy, which can be exploited, for example, in the removal of pollutants, or in the production of hydrogen or electricity<sup>14</sup>; a considerable and authoritative review can be found in reference **15**. The surface structure is central to its activity in this respect – some (surfaces) are relatively inactive while others are highly reactive. This has prompted many researchers to characterise the surface structure<sup>16</sup>, correlate with the activity<sup>17,18,19</sup> and selectively fabricate active morphologies<sup>20</sup>. The ability to design  $\text{TiO}_2$  nanocrystals that expose a high proportion of more active surfaces via synthetic control<sup>21</sup> has reignited the intense activity in this area. Indeed, even the possibility of inducing phase transitions by changing the surface chemistry has been proposed<sup>22</sup>. Clearly, full atomistic models for  $\text{TiO}_2$  nanocrystals would provide a valuable reference for understanding the chemical and physical properties of  $\text{TiO}_2$  nanomaterials and work in achieving this is well underway<sup>23,24</sup>.

Generating the full atomistic structure of a model nanocrystal is not a trivial undertaking – it is difficult to cleave it from the ‘bulk’ parent material because one is required to decide upon a multitude of variables. These include, for example, the morphology – i.e. which surfaces will be exposed, the structure of edges and vertices (where two or three surfaces meet respectively), the inclusion of point or extended defects including vacancies, interstitials dislocations and grain-boundaries. Conversely, Nature does not really suffer this problem because fabrication of a material experimentally inevitably involves some kind of ‘crystallisation’ process. Indeed, crystallisation processes influence the (micro)structure and hence the properties of the

material. Moreover, by modifying the crystallisation process (whether crystallisation from flame, solution, vapour deposition, molecular beam epitaxy, ball milling etc.) one can exert some control over the microstructure and hence the properties of the material facilitating the tantalising prospect of intelligent design of nanomaterials with desirable properties. One way of capturing, within a single atomistic model, the microstructural features observed experimentally, is to simulate the crystallisation process itself. Indeed, there have been many theoretical studies that attempt this. For example Gale and co-workers performed some highly detailed MD simulations on the growth and dissolution of urea crystals<sup>25,26</sup>. Similarly, Hamad et al. used MD to explore the embryonic stages of ZnS nanobubbles<sup>27</sup>. Here we take a similar approach and generate a full atomistic model of a TiO<sub>2</sub> nanocrystal by simulating TiO<sub>2</sub> crystallisation, under high-pressure, starting from an amorphous precursor<sup>28</sup>.

## **2. THEORETICAL METHODS**

In this section we describe the simulation code used to perform all the molecular dynamics (MD) simulations, the potential models that describe the interactions between the component ions, Ti, O and ‘Gas’ atoms, and finally, the procedure and conditions used to simulate the crystallisation of a TiO<sub>2</sub> nanocrystal resulting in a full atomistic structural model.

### **2.1 Simulation code**

The DL-Poly code was used to perform all the MD simulations<sup>29</sup>. This code utilizes three-dimensional periodic boundary conditions and therefore the nanocrystal was placed in the centre of a 3D periodic box, which was sufficiently large to ensure that the interactions between its neighbouring images were negligible.

## 2.2 Potential models

The Born model of the ionic solid was used to describe the  $\text{TiO}_2$  in which the component Ti and O ions interact via short-range parameterised interactions coupled with long-range Coulombic interactions. ‘Gas’ atoms were described using only a repulsive interaction to eliminate any possibility of the gas atoms crystallising. Parameters derived by Matsui and Akoagi<sup>30</sup> were chosen because they have been shown to predict morphologies for  $\text{TiO}_2$  rutile and anatase phases in accord with experiment<sup>31</sup>; the parameters are presented in table I and were used throughout this present study.

**Table I** Interatomic potentials of the form  $V(r) = A \exp(-r/\rho) - Cr^{-6}$ ; all other interactions are set to zero. G are gas ‘atoms’.

	A, eV mol <sup>-1</sup>	$\rho$ Å	C eV mol <sup>-1</sup> Å <sup>-6</sup>
Ti-O	16957.530	0.1940	12.5900
O - O	11782.760	0.2340	30.2200
Ti-Ti	31120.200	0.1540	5.2500
G - O	1000.0	0.5	0
G - G	1000.0	0.5	0
G - Ti	1000.0	0.5	0
Ionic charge	G = 0; Mass = 8	Ti = 2.196	O = -1.098

## 2.3 Nanocrystal generation

To crystallise a nanocrystal under pressure, the  $\text{TiO}_2$  nanoparticle was surrounded by a monatomic ‘gas’. In particular, a simulation cell was constructed, which comprised the  $\text{TiO}_2$  nanoparticle and ‘gas atoms’, fig. 1. To the left of the simulation cell, fig. 1(a), 15972 ions comprising the  $\text{TiO}_2$  nanoparticle (5324  $\text{Ti}^{4+}$  and 10648  $\text{O}^{2-}$  species) are shown, and to the right, 15972 gas atoms are included. To fill the simulation cell with an even distribution of gas atoms, repulsive interactions were assigned to act between the gas atoms and all other species - as described by the potential form given in table I; zero charges was assigned to gas atoms to prevent, at any pressure, electrostatic attraction and therefore eliminate the possibility of the gas crystallising.

Initially, the ions comprising the  $\text{TiO}_2$  were held fixed and only the gas atoms were allowed to move and, under MD performed at high temperature, the gas atoms started to repel one another and start to fill the (vacuum) space around the nanocrystal. When gas atoms approached the nanocrystal they were repelled in a similar fashion, which prevented any gas atoms from moving into the space occupied by the nanoparticle. Eventually, the system comprised a homogenous gas surrounding the  $\text{TiO}_2$  nanoparticle. The behaviour is shown graphically in fig. 1(a-c).

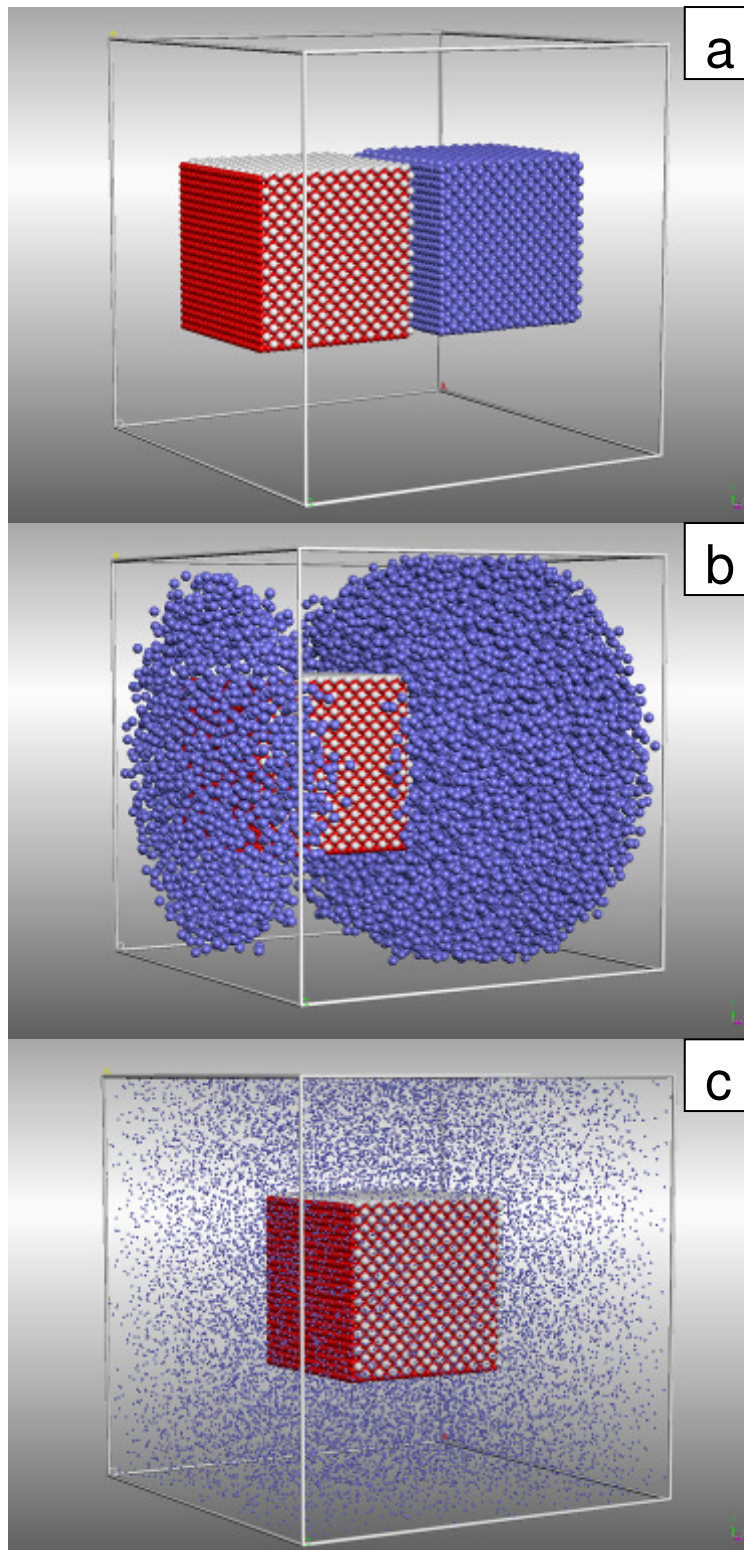


**Fig. 1** Encapsulation of the TiO<sub>2</sub> nanocrystal with ‘gas’ atoms. (a): starting configuration; (b): after 1ps of MD simulation; (c): after 5ps of MD simulation. Ti ions are represented by white spheres, the red spheres are oxygen and the blue spheres, gas atoms. In (c), the size of the gas atoms are reduced to enable the TiO<sub>2</sub> nanoparticle to be seen when completely surrounded by gas atoms.

Next, the pressure acting upon the  $\text{TiO}_2$  was increased and the nanoparticle was melted by increasing the temperature. The molten nanocrystal, fig. 2, adopts a spherical morphology - driven in an attempt to reduce its surface energy by minimising the surface area exposed. Finally, the nanoparticle was crystallised (under high pressure) by performing MD at reduced temperatures, annealed and then quenched to 10K; simulation details of each step are given in table II.

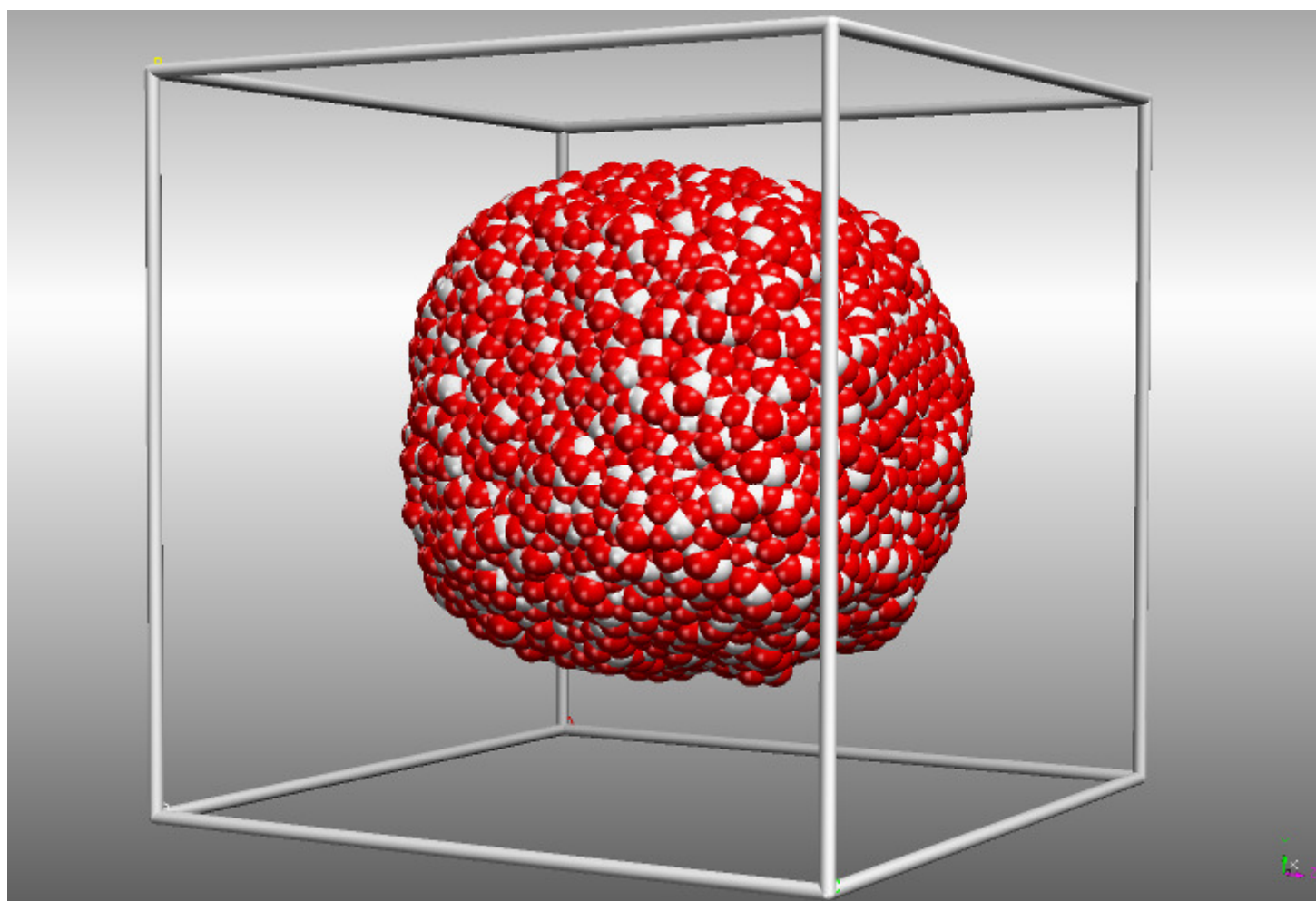


**Fig. 2** Sphere model representation of the atom positions comprising the molten  $\text{TiO}_2$  nanoparticle; the gas atoms are not shown. The white and red spheres correspond to titanium and oxygen respectively.

**Table II** Procedures and simulation conditions used to generate the TiO<sub>2</sub> nanocrystal

Aim	Ensemble	Temperature (K)	Time (ps)	Pressure (GPa)	Notes
1/ Encapsulate with gas	Constant volume	5000	5	-	Fig. 1; Ti and O ions held fixed
2/ Pressurise	Constant pressure	3000	12	20	Ti and O ions allowed to move
3/ Melt	Constant pressure	6000	28	20	Fig. 2
4/ Crystallisation	Constant pressure	2000	3682	20	Fig 3, fig 4
5/ Crystallisation	NPT	2000	1700	20	Thermostat and barostat relaxations set at 1ps
6/ Remove pressure	Constant volume	2000	3275	0	Gas atoms removed
7/ Anneal	NVT	1500	3700	0	250ps equilibration
8/ Quench	NVT	1000	250	0	250ps equilibration
	NVT	500	250	0	250ps equilibration
	NVT	10	250	0	250ps equilibration

### 3. RESULTS

In the first section, we describe the crystallisation process and then characterise the final low (10K) temperature atomistic structure.

#### 1.1. Crystallisation

The (high-pressure) crystallisation was monitored by animating the trajectories of the ions, during the MD simulation, using molecular graphics. At the start of the simulation, the nanoparticle is amorphous, fig. 3(a, b). However, at some point during the MD simulation, a crystalline ‘seed’ evolves and the oxygen and titanium species, comprising the amorphous sea of ions surrounding the seed, start to condense onto its surface, propagating its size. Fig. 3(c) reveals that two crystalline ‘seeds’ have evolved and both start to grow, fig. 3(d). These crystalline regions are similar in structure (although they appear different in the figure because they are misoriented with respect to one another). As the two crystalline regions continue to grow, they impinge upon one another, fig. 3(e), resulting in the formation of a grain-boundary, 3(f).

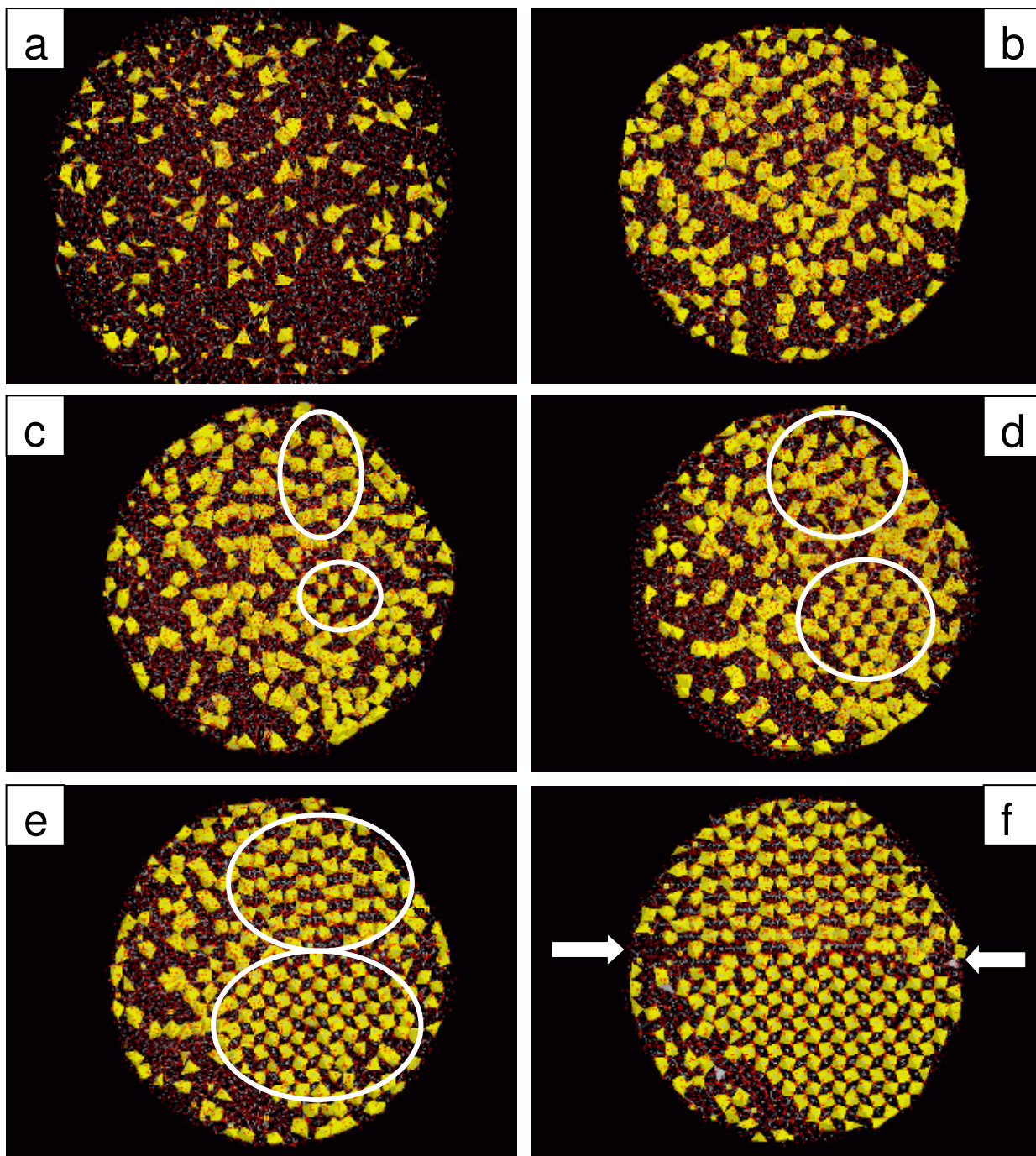


**Fig. 3** Snapshots of the nanoparticle taken at various time intervals during the simulated crystallisation illustrating (a): the amorphous starting configuration (0ps); (b): the molten nanoparticle, which accommodates a spherical morphology (200ps); (c): the evolution of two crystalline seeds (1000ps); (d) growth of the crystalline regions (1200ps); (e) point at which the two grains start to impinge on one another resulting (because the two grains are misaligned) in the formation of a grain-boundary (1500ps); (f): system after 3500ps at which point the system is no longer undergoing significant structural change. The arrows indicate the grain-boundary. The yellow polyhedra comprise a central, octahedrally coordinated Ti ion surrounded by a shell of six oxygens. To facilitate clarity of the figure only those octahedrally coordinated Ti ions within a thin slice through the nanoparticle are shown. The figure therefore necessarily depicts a two-dimensional representation of a (three-dimensional) crystallisation.

The configurational (system) energy<sup>29</sup>, calculated from the beginning of the crystallisation step, is shown in fig. 4. The energy reduces (a lower energy corresponds to a more stable structural configuration) until about 3000ps at which point it starts to converge. The drop in energy reflects the latent heat of crystallisation, which can easily build up and reamorphise the nanocrystal. Accordingly, to quickly extract this energy from the system, the velocities were scaled to the simulation temperature every timestep (0.005ps).

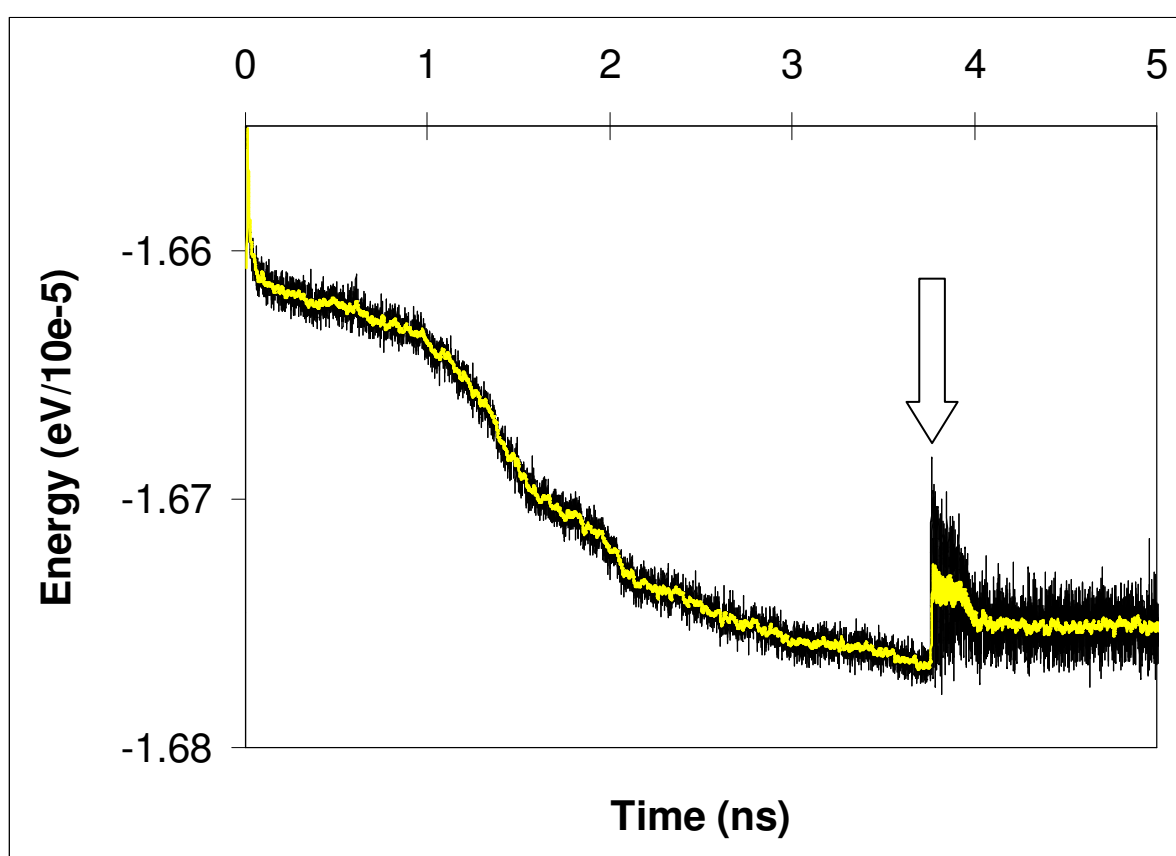


**Fig. 4** Configurational energy, calculated as a function of time during the crystallisation; a more negative energy corresponds to a more stable structure. The arrow indicates the point at which velocity scaling to the simulation temperature at every timestep was discontinued and replaced by a thermostat and barostat. A moving average trendline (yellow) helps guide the eye and reduce the effect of the energy fluctuations. This figure is usefully compared with snapshots of the structure taken during the crystallisation in fig. 3.

A more realistic method of extracting the heat of crystallisation from the system is via thermostat and barostat with relaxation times of about 1ps. However, this was not pursued because of the prohibitively high computational costs associated with determining adequate conditions to facilitate crystallisation (without the nanocrystal reamorphising); each 1000ps of MD simulation requires 10 hours using 96 processors of a Sun Galaxy-class configuration supercomputer. To support this decision, we found, in a previous study, that a full crystallisation performed with the heat of crystallisation extracted via thermostat and barostat (1ps relaxation time) resulted in a final configuration that was structurally equivalent to the system where the velocities of the ions were scaled to the simulation temperature every timestep<sup>32</sup>. Accordingly, we suggest that scaling every timestep is a valid, albeit less realistic, approach.

In this present study, temperature scaling was applied every timestep for the first 3682ps after which the latent heat of crystallisation was extracted via thermostat and barostat (1ps relaxation time). In fig. 4, one can see the increased fluctuations in the configuration energy after the velocity scaling is switched off. It is clear from fig. 4 that the configurational energy has converged completely after about 5000ps.

## **1.2. Atomistic crystal structure**

The final, low temperature (10K) structure of the TiO<sub>2</sub> nanocrystal is shown in fig. 5. The nanocrystal is not a single crystal; rather it comprises three misoriented grains. Molecular graphics was then used extensively to help determine the atomistic structure of the nanocrystal.

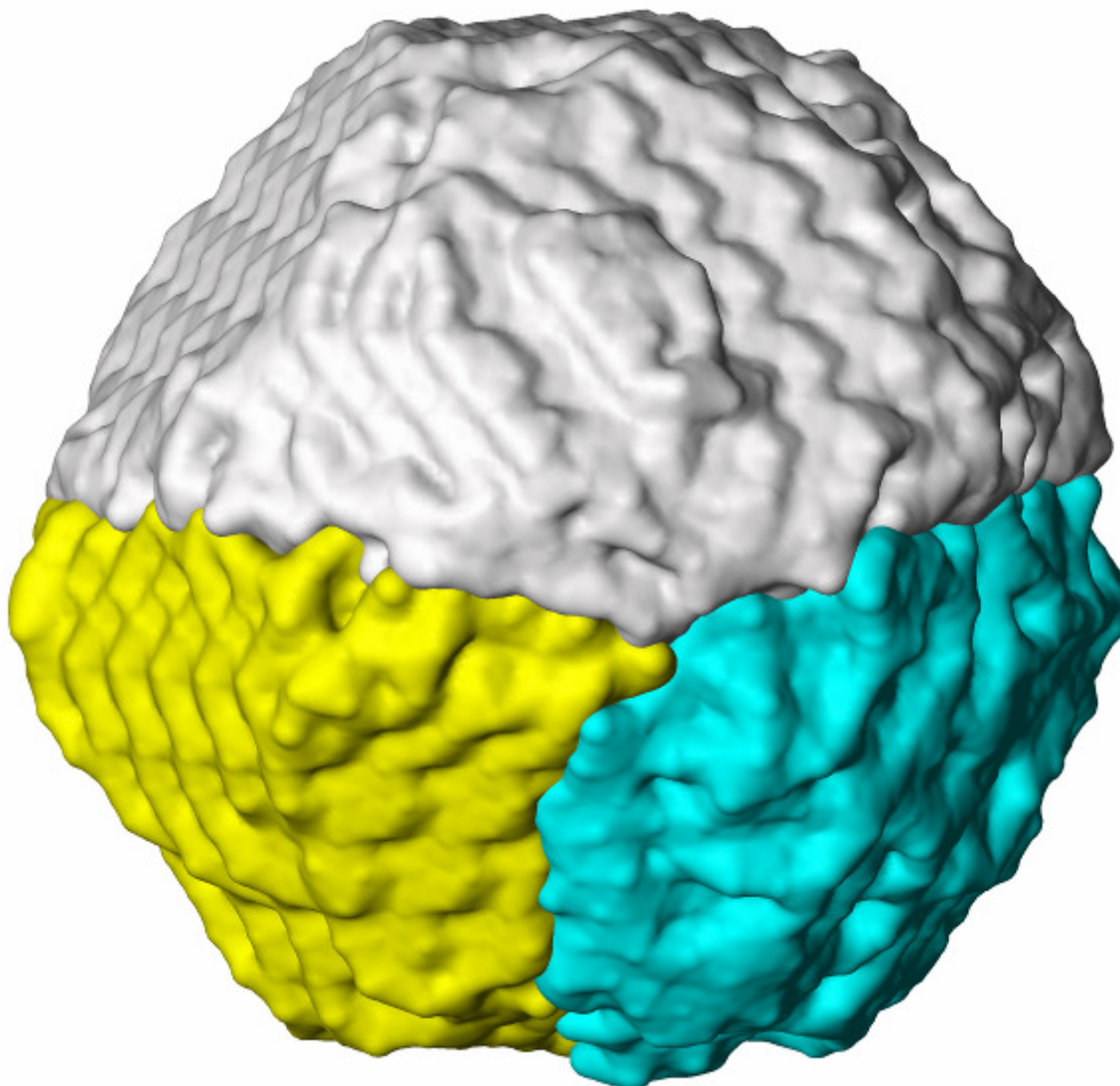


**Fig. 5** Final, low temperature, structure for the  $\text{TiO}_2$  nanocrystal shown with surface rendering. The colours correspond to the three individual grains comprising the nanocrystal.

In fig. 6(a), a thin slice, cut through the nanocrystal, is shown, revealing three grains separated by (three) grain-boundaries and a grain-junction. The top grain conforms to the  $\alpha\text{-PbO}_2$  structure<sup>33</sup>. An enlarged segment of this grain, showing the characteristic zig-zag filling of the octahedral sites by Ti to facilitate the  $\alpha\text{-PbO}_2$  structure, is presented in fig. 6(b). The grain, bottom left of fig. 6(a), also accommodates the  $\alpha\text{-PbO}_2$  structure but includes a rutile-structured intergrowth, which can be distinguished from the  $\alpha\text{-PbO}_2$  domain, by noting the straight filling of the octahedral sites by Ti associated with rutile structure.

**Fig. 6** Molecular graphics representation of the atom positions comprising the nanocrystal. (a): slice cut through the nanocrystal showing the interconnecting grains. The oxygen ions are removed and the Ti ions (blue) are connected to aid visualisation. (b) segment of (a) depicting the zig-zag filling by Ti of the octahedral sites between the oxygen layers. The oxygen layer above the plane of the paper are coloured yellow, and the oxygen plane below the plane of the page are coloured red; titanium are blue. (c) segment, bottom left, of (a) showing a domain conforming to the rutile structure. The inset was constructed using crystallographic coordinates taken from the (perfect) parent material. Titanium is blue and oxygen, red. (d) segment, bottom right, of (a) showing the zig-zag ( $\alpha$ -PbO<sub>2</sub>) and straight (rutile) domains comprising the nanocrystal. Ti are coloured blue (above the plane of the paper) and grey (below the plane).

Inspection of a segment of the rutile intergrowth, fig. 6(c), reveals it to be heavily distorted (a perfect rutile structure is inset in fig. 6(c) to compare). An enlarged segment of the third grain, fig. 6(a) bottom right, is shown in fig. 6(d). This region also comprises  $\alpha$ -PbO<sub>2</sub> and rutile-structured domains. When the domains are this small (pertinent to nanocrystals) it is difficult to decide whether the nanocrystal comprises rutile and  $\alpha$ -PbO<sub>2</sub> microdomains or the rutile is simply heavily twinned or, conversely it conforms to the  $\alpha$ -PbO<sub>2</sub> structure but includes stacking faults.

It is perhaps not surprising that the nanocrystal evolved domains conforming to the  $\alpha$ -PbO<sub>2</sub> structure because this structure has been observed as a high-pressure polymorph of TiO<sub>2</sub><sup>34</sup>. In particular, as the pressure is increased, TiO<sub>2</sub> transforms from rutile to  $\alpha$ -PbO<sub>2</sub> to Baddeleyite<sup>35</sup>. We note that our simulated crystallisation procedure does not require or indeed allow the manual construction (i.e. via symmetry) of the  $\alpha$ -PbO<sub>2</sub> phase; rather the crystalline structure must evolve ‘naturally’, from the amorphous (molten) precursor. In addition, within the amorphous-crystalline transformation, Ti-O distances will necessarily span a wide range. Clearly, this represents a stringent validation of both the potential model and the simulation strategy in that it can evolve realistic structures of nanocrystals including experimentally determined polymorphs at high pressure.

After identifying the  $\alpha$ -PbO<sub>2</sub>-structured TiO<sub>2</sub>, it was deemed useful to determine how well the potential model, table I, performs in reproducing the parent (bulk) material. To this end, TiO<sub>2</sub>, isostructural with  $\alpha$ -PbO<sub>2</sub>, was generated from single crystal diffraction data of  $\alpha$ -PbO<sub>2</sub><sup>33</sup> and energy minimised using the *gulp* code<sup>36</sup>.

Predicted cell parameters and bond distances are presented in table III together with experimental data for rutile and  $\alpha$ -PbO<sub>2</sub>; nearest neighbour distances for the nanocrystal were determined from calculated radial

distribution functions, fig. 7. The potential model can be seen to describe the rutile and  $\alpha$ -PbO<sub>2</sub> polymorphs in good agreement with experiment.

**Table III** Experimentally and theoretically determined structural parameters for TiO<sub>2</sub> (rutile and  $\alpha$ -PbO<sub>2</sub> polymorphs) bulk parent material and nanocrystal.

	a	b	c	Ti-O distance (Å)	Reference
<b>TiO<sub>2</sub> (Rutile)</b>					
<i>Energy Minimisation</i>	4.493		3.009	1.956(4x), 1.927(2x)	<i>This work</i>
DFT	4.572		2.926	1.934(4x), 1.968(2x)	<b>37</b>
EXPERIMENT	4.586		2.958	1.946(4x), 1.976(2x)	<b>38</b>
<b>TiO<sub>2</sub> (<math>\alpha</math>-PbO<sub>2</sub>)</b>					
<i>Energy Minimisation</i>	4.522	5.379	4.936	1.914(2x), 1.951(2x), 1.985(2x)	<i>This work</i>
DFT	4.535	5.447	4.858	1.862(2x), 1.938(2x), 2.067(2x)	<b>37</b>
EXPERIMENT	4.541	5.493	4.906		<b>39</b>
<b>Nanocrystals</b>					
<i>MD(<math>\alpha</math>-PbO<sub>2</sub>)</i>				1.93 (range: 1.8-2.1)	<i>This work</i>
MD(Rutile)				1.920	<b>40</b>
MD(Anatase)				1.945	<b>40</b>
EXPERIMENT ( $\alpha$ -PbO <sub>2</sub> )	4.61	5.43	4.87		<b>41</b>

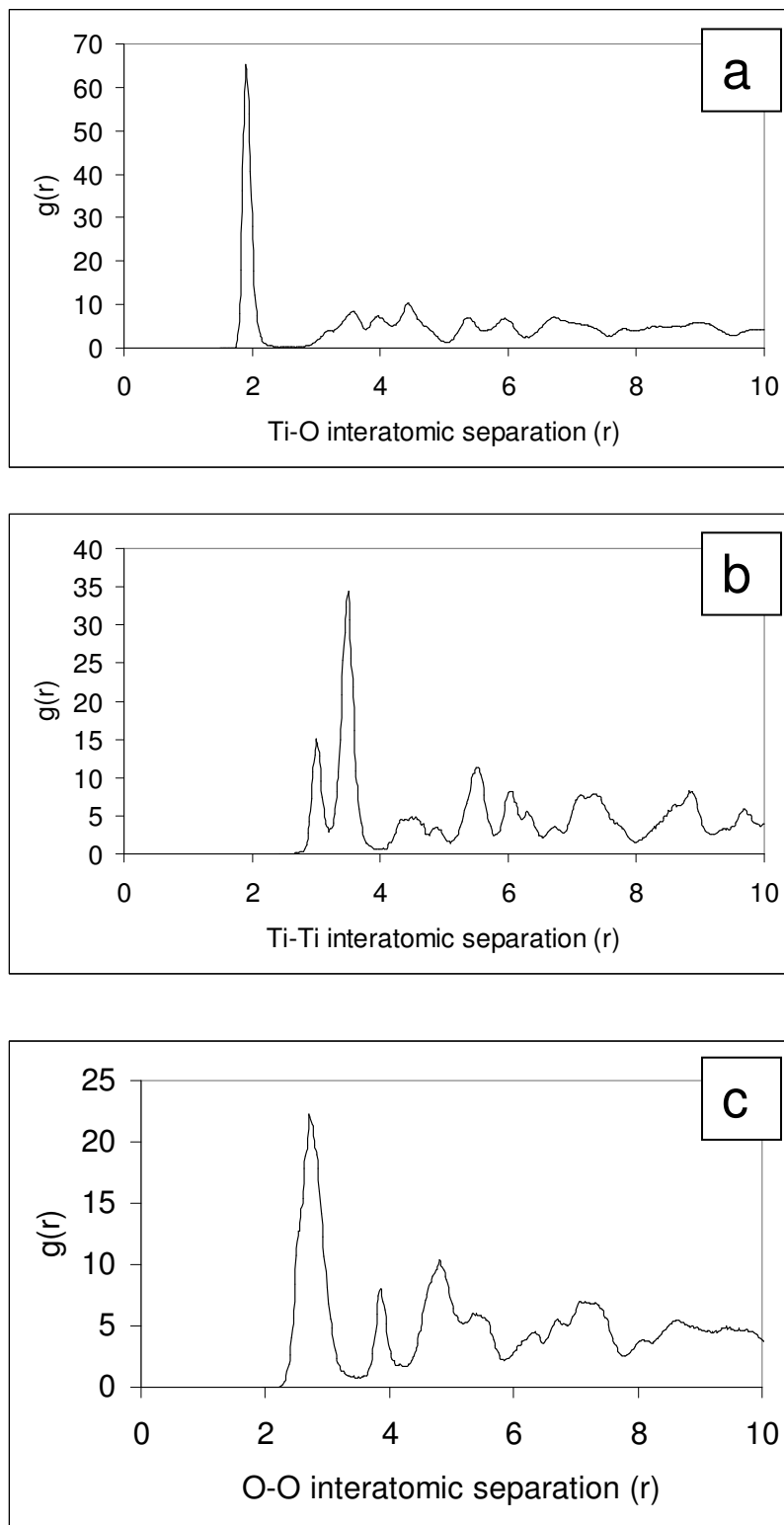


**Fig. 7** Calculated (a): Ti-O; (b): Ti-Ti and (c): O-O radial distribution functions.

## 2.3 Microstructure

In this section, we explore the microstructural features that have evolved; these include the morphology and surface structures, dislocations and grain-boundaries, isolated and associated point defects such as vacancies and interstitials and the packing of the oxygen sublattice.

### 2.3.1 Morphology

To help determine the morphology of the nanocrystal and characterise the surfaces exposed, a slice was cut through the nanocrystal and is shown in fig. 8(a). Inspection of the slice reveals two relatively flat surfaces that appear to be (001) and (111); the insets, bottom left and bottom right, depict the perfect (111) and (001) surfaces, which have been cleaved from the parent (bulk) material to compare.

In fig. 9, three views (a-c) of the nanocrystal are shown and reveal a truncated polyhedral morphology. The small size of the nanocrystal (about 7nm) necessarily results in a high concentration of edges (where two surfaces meet) and corners (where three surfaces meet); the edges and corners are not atomically sharp. In addition, some of the surfaces are stepped and exhibit slight curvature of the surface plane. Coupled with extensive relaxation of the surface and near surface ions, characterisation, by assigning a particular Miller index, is difficult. Nevertheless, we have described three surfaces in fig. 9 as conforming to (111), (010) and (001). However, for the reasons stated above these assignments should be treated with a degree of caution.

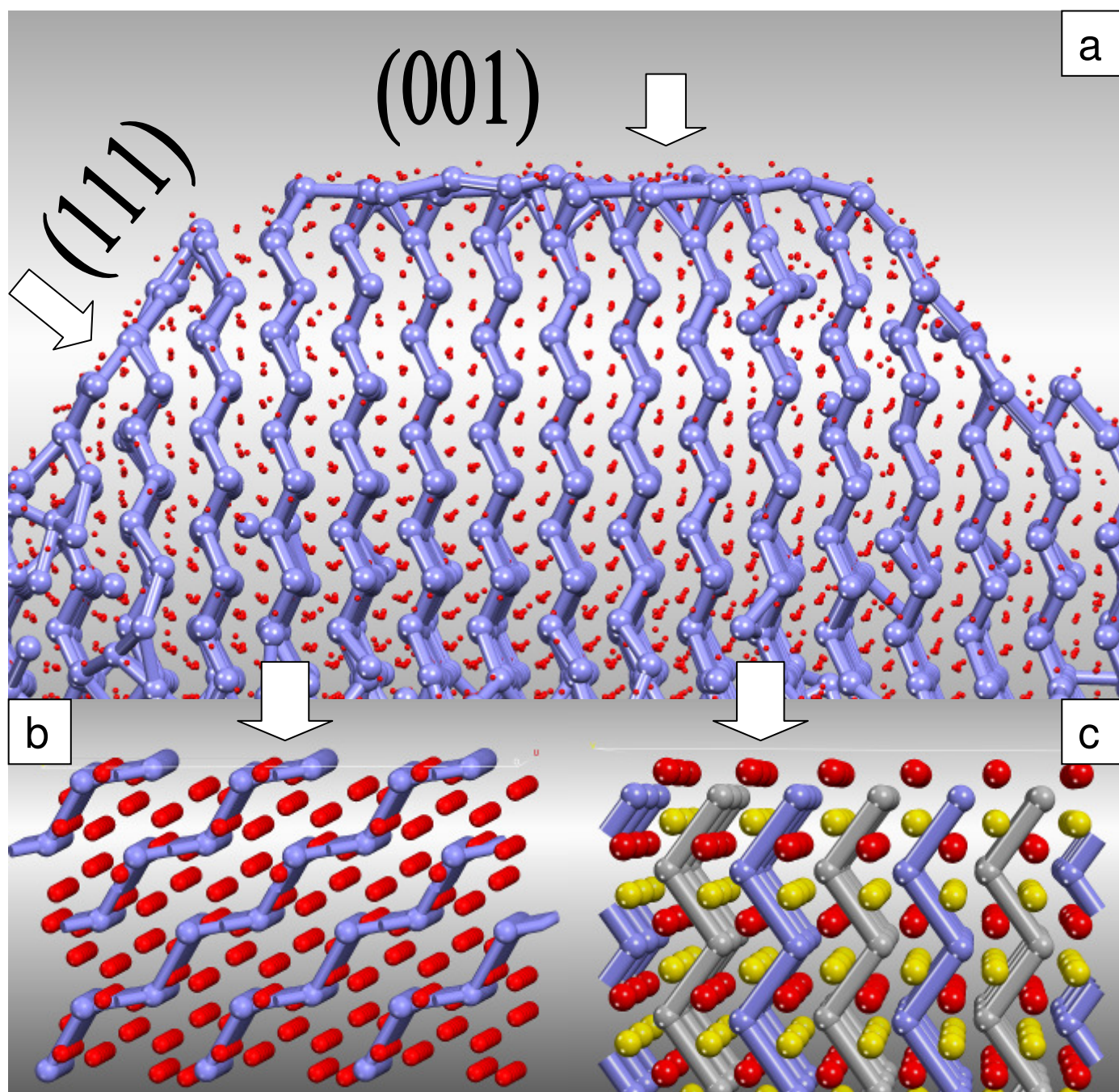


**Fig. 8** Segment of the TiO<sub>2</sub> nanocrystal depicting the (001) and (111) surfaces exposed compared with analogous surfaces cut from the perfect (PbO<sub>2</sub>-structured) parent material. The arrows indicate the surfaces. (a): segment of the nanocrystal; (b): parent material depicting the (111) surface (top); (c) parent material showing the (001) surface (top). Titanium is blue (or grey) and oxygen is red (or yellow) – colour notation is used to help describe the structure more clearly.

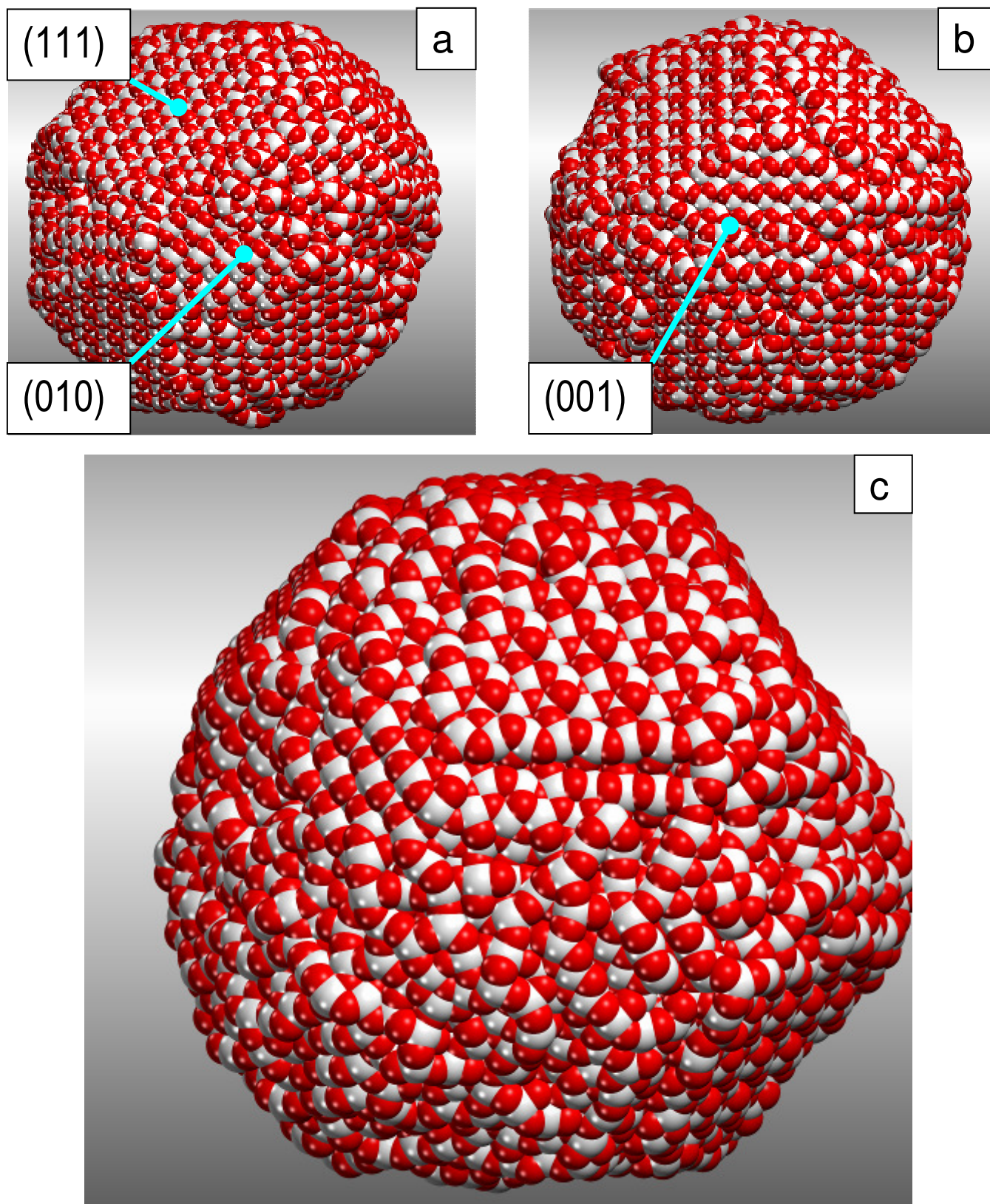


**Fig. 9** Sphere model representation of the  $\text{TiO}_2$  nanocrystal shown with different orientations - (a), (b) and (c) - to help describe the three-dimensional structure and the configuration of the (111), (010) and (001) surfaces. Oxygen is red and titanium, white.

Experimentally,  $\text{TiO}_2$  nanocrystals with  $\alpha\text{-PbO}_2$  structure have been fabricated using laser ablation condensation<sup>40</sup>. The authors did not observe impurities within the nanocrystals, which may have accounted for the  $\alpha\text{-PbO}_2$  structure; rather they attributed the evolution and stabilisation of this (high-pressure) phase to the combined effects of rapid heating and cooling and the nanometer-size effect with respect to minimisation of the surface energy compared with the rutile polymorph. The authors also identify  $(1\bar{1}0)$ ,  $(010)$  and  $(001)$  facets for 10nm particles and spherical morphology for particles about 1000nm in size; in this study we observe  $(010)$ ,  $(001)$ , fig. 9, and, after careful inspection, we have been able to identify a small region corresponding to the  $(1\bar{1}0)$  surface.

Kuo et al. have calculated the energies of low index surfaces of  $\alpha\text{-PbO}_2$ -structured  $\text{TiO}_2$  and find they decrease in the order:  $(100) > (001) > (110) > (010)$ ,<sup>42</sup>, where the  $(010)$  is calculated to have the lowest energy and is therefore deemed the most stable surface.

### 2.3.2 Grain-boundaries, grain-junction

In fig. 10 an enlarged view of the slice, fig. 6(a) is shown revealing more clearly the grain-boundaries and grain-junction between the three misoriented grains. The grain-boundaries are indexed as A:  $(001)/(001)$  twist boundary - the top grain is rotated by about  $30^\circ$ ; B: top $(001)$ /bottom $(111)$  twist boundary; C: left $(010)$ /right $(111)$ . Inspection of the structure using molecular graphics reveals that the grain-boundary planes are curved rather than flat and therefore our assignments of the grain-boundary indices are necessarily approximate and should, similar to our surface assignments, be treated with a degree of caution.

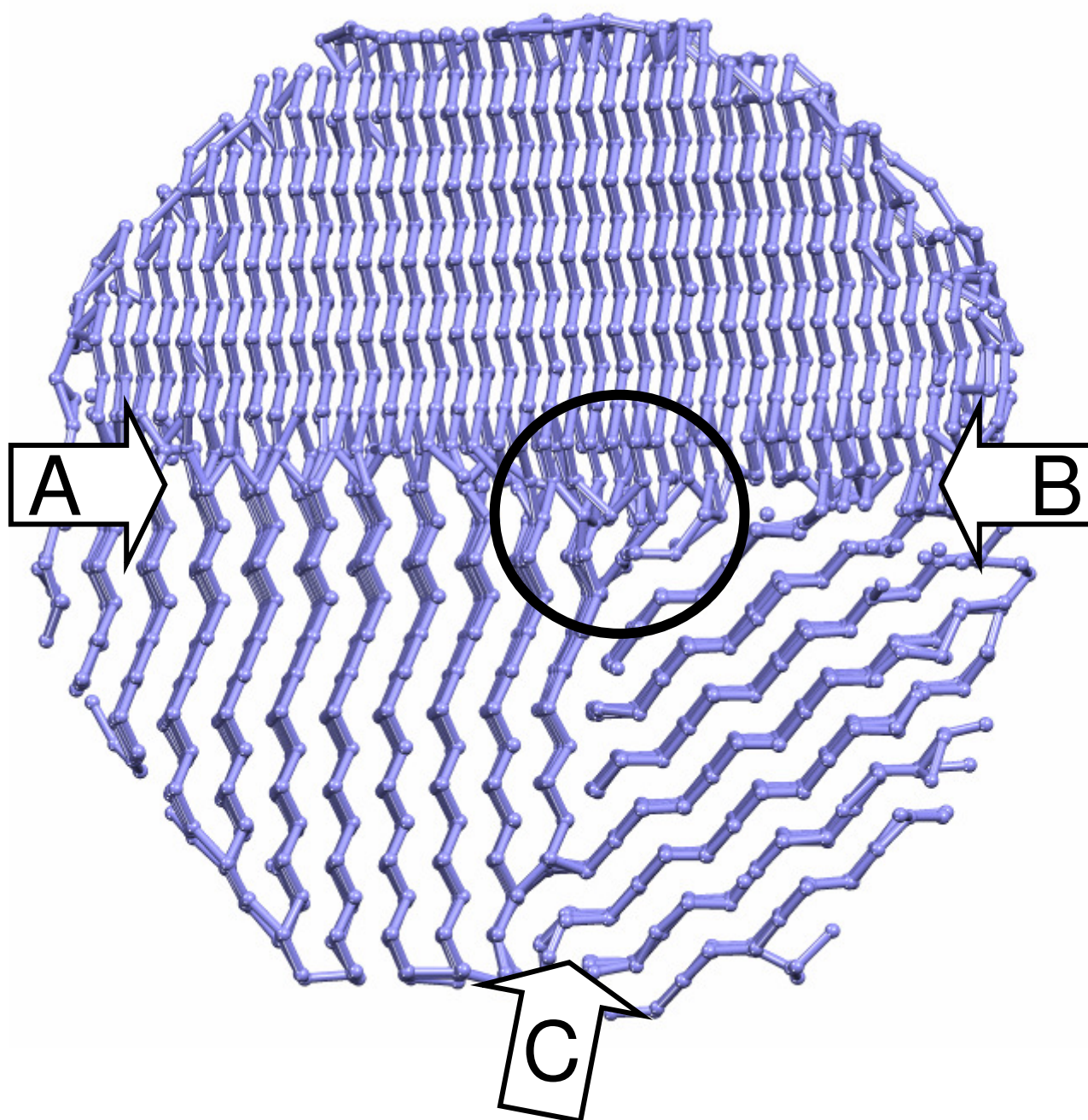


**Fig. 10** Stick model representation of the titanium ions comprising the TiO<sub>2</sub> nanocrystal. The oxygen ions have been omitted to reveal more clearly the three grain-boundaries (indicated by the arrows and labeled A: (001)/(001) twist-boundary (approximately 30°); B: top(001)/bottom(111) twist-boundary, C: left(010)/right(111) and the grain junction structure, which is circled.

### 2.3.3 Oxygen Packing

Packing of oxygen sublattice is approximately (they are distorted) hexagonal close packed or ‘ABABAB’ stacking of the oxygen in both the  $\alpha$ -PbO<sub>2</sub> and rutile domains. We note that in previous simulations on MnO<sub>2</sub> nanocrystals, the atomistic model comprised a mixture of both ‘ABCABC’ (cubic close packed) and ‘ABABAB’ stacking of the oxygen sublattice<sup>32</sup>.

### 2.3.4 Point Defects

Careful analysis of the nanocrystal revealed no point defects within any of the three crystallites other than at surface or interface regions; surface and interface structures are difficult to characterise because of the considerable ionic relaxation. This is perhaps surprising because in previous studies we have noted that the high speed of crystallisation, associated with these simulations results in a high concentration of isolated and associated point defects<sup>28</sup>. We suggest, tentatively, that the (very high) pressure imposed upon the system was sufficient to eliminate any point defects such as vacancies or interstitials as they evolved. It is possible to analyse the trajectories or animations of all the ions during the crystallisation to determine whether this is the case although we note this is not a trivial undertaking because the trajectory files, corresponding to the crystallisation, are of the order of terabytes in size and therefore we will explore this possibility in a future study when suitably large storage facilities become available.

## 4. CONCLUSIONS

A strategy has been devised to generate full atomistic models of nanocrystals by simulating crystallisation at high-pressure starting from a molten precursor. In particular, a molten TiO<sub>2</sub> nanoparticle was generated at

6000K and then crystallised at 2000K under 20GPa pressure. This approach negates the need for any prior structural data i.e. crystal structure, morphology, surface Miller indices, intrinsic defect etc.; rather the system evolves in response only to the simulation conditions such as temperature, pressure and the potential model that describes the interactions between species comprising the system.

The simulation procedure was tested using  $\text{TiO}_2$  as a model system because of the rich variety of pressure related polymorphs it accommodates, including: rutile, anatase, fluorite, brookite,  $\alpha\text{-PbO}_2$ , baddeleyite, cotunnite<sup>43</sup>. The (final) structure of the simulated nanocrystal comprised rutile- and  $\alpha\text{-PbO}_2$ -structured  $\text{TiO}_2$ ; the latter is known as a high pressure phase of  $\text{TiO}_2$ . The nanocrystal expressed well-defined facets including (111), (010) and (001) and a small region corresponding to  $(1\bar{1}0)$ . Microstructural features include three grain boundaries conforming to (001)/(001) 30° twist, (001)/(111) twist and (010)/(111) and a grain-junction between the three. Analysis of the nanocrystal did not reveal the presence of intrinsic point defects (vacancies, interstitials) other than at grain-boundary or surface regions. This was attributed (tentatively) to the annealing out of any defects as they formed because of the high-pressure conditions imposed upon the system during crystallisation although further work is needed to confirm this proposition.

Experimentally, nanocrystals of  $\text{TiO}_2$  with  $\alpha\text{-PbO}_2$  structure, have been synthesised using laser ablation condensation and were found to expose (010), (001) and  $(1\bar{1}0)$  facets, which helps validate our simulation approach and the resulting structural model.

Simulating crystallisation is a stringent test of the potential model. Moreover, that the approach yielded not only the correct structure (i.e. rutile) from an amorphous or molten precursor, but also the high pressure phase ( $\alpha\text{-PbO}_2$ ) together with morphological features (surface Miller indices in accord with experiment) and

microstructural features that are realistic, such as grain-boundaries and grain-junction, inspires confidence in that the approach is able to simulate, in part, crystallisation at high-pressure in a real system. Accordingly, we suggest that this technique can be used for generating other oxide nanocrystals under conditions of high temperature and pressure starting from an amorphous precursor and may prove applicable to other materials such as metals or semiconductors.

Full atomistic models of nanocrystals are valuable because they can be used, for example: to complement or help rationalise experimental data including, for example, x-ray diffraction<sup>24</sup> and electron microscopy data<sup>44</sup>; calculate pertinent properties such as oxygen vacancy formation<sup>1</sup> oxygen transport or extrinsically doped with implications for fuel cells and catalysis<sup>45</sup>; starting configurations for computationally more intensive quantum mechanical calculations to explore electronic properties such as surface reactivity<sup>46</sup>; interaction studies with other materials such as polymers – with implications for coating technologies; building blocks to explore mechanisms for aggregation or dispersion to form ordered arrays; help guide synthetic strategies to fabricate a particular (desirable) size and shape of nanocrystal. To this end we have deposited the coordinates of all the atom positions comprising this TiO<sub>2</sub> nanocrystal to the journal as supplementary material. Ultimately, atomistic models will help experiment unravel the profound influence (structural, property and application) of traversing to the nanoscale.

**Acknowledgements:** Financial support from EPSRC(EPSRC (GR/S48431/1 and GR/S48448/01) for funding one of us (TXTS), Cambridge-Cranfield HPCF for computational facilities and EPSRC (GR/S84415/01) for computational facilities.

## References

---

- [1]. T. X. T. Sayle, S. C. Parker and D. C. Sayle, *J. Phys. Chem. Chem. Phys.* 7, 2936 (2005).
- [2]. T. X. T. Sayle, S. C. Parker and C. R. A. Catlow, *Surface Science* 316, 329 (1994).
- [3]. H. X. Mai, L. D. Sun, Y. W. Zhang, R. Si, W. Feng, H. P. Zhang, H. C. Liu and C. H. Yan, *J. Physical Chemistry B* 109, 24380 (2005).
- [4]. K. J. Rao, K. Mahesh and S. Kumar, *Bulletin of Materials Science* 28, 19 (2005).
- [5]. S. O'Brien, L. Brus and C. B. Murray, *J. Amer. Chem. Soc.* 123, 12085 (2001).
- [6]. X. H. Liu, C. Kan, X. Wang, X. J. Yang and L. D. Lu, *J. Amer. Chem. Soc.* 128, 430 (2006).
- [7]. N. G. Glumac, G. Skandan, Y. J. Chen and B. H. Kear, *Nanostructured Materials* 12, 253 (1999).
- [8]. P. F. Mc Millan, *Nature Materials* 1, 19 (2002).
- [9]. P. F. Mc Millan, *J. Materials Chemistry* 14, 1506 (2004).
- [10]. P. F. Mc Millan, *Nature Materials* 4, 715 (2005).
- [11]. V. Swamy, A. Kuznetsov, L. S. Dubrovinsky, P. F. McMillan, V. B. Prakapenka G. Shen and B. C. Muddle *A. Phys. Rev. Lett.* 96(13), Art. No. 135702 (2006).
- [12]. N. K. Bourne, *Measurement Science and Technology* 14, 273 (2003).
- [13]. V. Swamy, A. Kuznetsov, L. S. Dubrovinsky, R. A. Caruso, D. G. Shchukin and B. C. Muddle *Physical Review B* 71 (18) Article 184302 (2005).
- [14]. S. U. M. Khan, M. Al-Shahry and W.B. Ingler, *Science* 297, 2243 (2002).
- [15]. U. Diebold, *Surface Science Reports* 48, 53 (2003).
- [16]. M. Y. Kuo, C. L. Chen, C. Y. Hua, H. C. Yang and P.Y. Shen, *J. Physical Chemistry B* 109, 8693 (2005).
- [17]. X. Q. Gong and A. Selloni, *J. Physical Chemistry B* 109, 19560 (2005).
- [18]. R. Schaub, E. Wahlstrom, A. Ronnau, E. Laegsgaard, I. Stensgaard and F. Besenbacher *Science* 299, 377 (2003).
- [19]. E. Wahlstrom, E. K. Vestergaard, R. Schaub, A. Ronnau, M. Vestergaard E., Laegsgaard, I. Stensgaard and F. Besenbacher, *Science* 303, 511 (2004).
- [20]. Y. Gao and S. A. Elder, *Materials Letters* 44, 228 (2000).
- [21]. T. Moritz, *European J. Inorganic Chemistry* 2, 235 (1999).
- [22]. A. S. Barnard and L. A. Curtiss, *Nano Letters* 5, 1261 (2005).
- [23]. S. Hamad, C. R. A. Catlow, S. M. Woodley, S. Lago and J. A. Mejias, *J. Physical Chemistry B* 109, 15741 (2005).
- [24]. P. K. Naicker, P. T. Cummings, H. Z. Zhang and J. F. Banfield, *J. Physical Chemistry B* 109, 15243 (2005).
- [25]. S. Piana, M. Reyhani and J. D. Gale, *Nature* 438, 70 (2005).
- [26]. S. Piana and J. D. Gale, *J. American Chem. Soc.* 127, 1975 (2005).
- [27]. S. Hamad, S. Cristol and C. R. A. Catlow, *J. American Chem. Soc.* 127, 2580 (2005).
- [28]. T. X. T. Sayle, C. R. A. Catlow, P. R. Maphanga, P. E. Ngoepe and D. C. Sayle, *J. American Chem. Soc.* 127, 12828 (2005).
- [29]. W. Smith and T. R. Forster, DL\_POLY is a package of Molecular Simulation routines written by Smith and Forester Copyright by the council for the Central Laboratory of the Research Councils, Daresbury Laboratory, Daresbury, Warrington, UK (1996) <http://www.dl.ac.uk/TCSC/Software/DLPOLY>.
- [30]. M. Matsui and M. Akaogi, *Mol. Simul.* 6, 239 (1991).

- 
- [31]. P. M. Oliver, G. W. Watson, E. T. Kelsey and S. C. Parker, *J. Materials Chemistry* 7, 563 (1997).
- [32]. T. X. T. Sayle, C. R. A. Catlow, P. R. Maphanga, P. E. Ngoepe and D. C. Sayle, *J. Crystal Growth*. In press (2006).
- [33]. S. Filatov, N. Bendeliani, B. Albert, H. Kopf, T. Dyuzeva and L. Lityagina, *Solid State Sciences* 7, 1363 (2005).
- [34]. T. Sasaki, *J. Physics – Condensed Matter* 14, 10557 (2002).
- [35]. S. L. Hwang, P. Y. Shen and T. F. Yui, *Science* 288, 321 (2000).
- [36]. J. D. Gale, *Zeitschrift Fur Kristallographie* 220, 552 (2005).
- [37]. M. Y. Kuo, C. L. Chen, C. Y. Hua, H. C. Yang and P. Y. Shen, *J. Physical Chemistry B* 109, 8693 (2005).
- [38]. J. K. Burdett, T. Hughbanks, G. J. Miller, J. W. Richardson and J. V. Smith, *J. American Chem. Soc.* 109, 3639 (1987).
- [39]. L. Gerward and J. S. Olsen, *J. Applied Crystallography* 30, 259 (1997).
- [40]. P. K. Naicker, P. T. Cummings, H. Z. Zhang and J. F. Banfield, *J. Physical Chemistry B* 109, 15243 (2005).
- [41]. S. Y. Chen and P. Y. Shen, *Phys. Rev. Letters* 89, Art. No. 096106 (2002).
- [42]. M. Y. Kuo, C. L. Chen, H. C. Yang, C. Y. Hua and P. Y. Shen, *Phys. Rev. B* 71, Art. No. 125405 (2005).
- [43]. V. Swamy, J. D. Gale and L. S. Dubrovinsky, *J. Physics and Chemistry of Solids* 62, 887 (2001).
- [44]. T. X. T. Sayle, S. C. Parker and D. C. Sayle, *J. Material Chemistry* 16, 1067 (2006).
- [45]. T. X. T. Sayle, S. C. Parker and D. C. Sayle, *Faraday Discussions*, In press (2006).
- [46]. M. Nolan, S. C. Parker and G. W. Watson, *J. Physical Chemistry B* 110, 2256 (2006).

# High-pressure crystallisation of TiO<sub>2</sub> nanoparticles

Sayle, Dean C.

2007-03-31T00:00:00Z

---

Sayle DC, Sayle TXT. (2007) High-pressure crystallisation of TiO<sub>2</sub> nanoparticles. Journal of Computational and Theoretical Nanoscience, Volume 4, Issue 2, April 2007, pp. 299-308

<https://doi.org/10.1166/jctn.2007.2319>

*Downloaded from CERES Research Repository, Cranfield University*